Thirty-minute plasma sustainment by real-time magnetic-axis swing for effective divertor-load-dispersion in the Large Helical Device[a)]

T. Mutoh,[b)] S. Masuzaki, R. Kumazawa, T. Seki, K. Saito, Y. Nakamura, S. Kubo, Y. Takeiri, T. Shimozuma, Y. Yoshimura, H. Igami, K. Ohkubo, T. Watanabe, H. Ogawa,[c)] J. Miyazawa, M. Shoji, N. Ashikawa, K. Nishimura, M. Sakamoto,[d)] M. Osakabe, K. Tsumori, K. Ikeda, H. Chikaraishi, H. Funaba, S. Morita, M. Goto, T. Tokuzawa, N. Takeuchi,[e)] F. Shimpo, G. Nomura, C. Takahashi, M. Yokota, Y. P. Zhao,[f)] J. G. Kwak,[g)] H. Yamada, K. Kawahata, N. Ohyabu, O. Kaneko, K. Ida, Y. Nagayama, N. Noda, A. Komori, S. Sudo, O. Motojima, and LHD Experiment Group
National Institute for Fusion Science, Oroshi-cho 322-6, Toki city 509-5292, Japan

(Received 24 October 2005; accepted 20 December 2005; published online 17 May 2006)

Achieving steady-state plasma operation at high plasma temperatures is one of the important goals of worldwide magnetic fusion research. A high temperature of approximately 2 keV, and steady-state plasma-sustainment operation of the Large Helical Device (LHD) [O. Motojima, K. Akaishi, H. Chikaraishi *et al.*, Nucl. Fusion **40**, 599 (2000)] is reported. High-temperature plasmas were created and maintained for more than 30 min with a world record injected heating power of 1.3 GJ. The three-dimensional heat-deposition profile of the LHD helical divertor was modified and during long-pulse discharges it effectively dispersed the heat load using a magnetic-axis swing technique developed at the LHD. A sweep of only 3 cm of the major radius of the magnetic axis position (less than 1% of the major radius of the LHD) was enough to disperse the divertor heat load. The modification of the heat-load profile was explained well by field-line tracing. The steady-state plasma was heated and sustained mainly by hydrogen minority ion heating using ion cyclotron range of frequencies. The operation lasted until a sudden increase of radiation loss occurred, presumably because of wall metal flakes dropping into the plasma. The sustained line-averaged electron density was approximately $0.7-0.8\times10^{19}$ m^{-3}. The average input power was 680 kW, and the plasma duration was 31 min 45 s. This successful long operation shows that the heliotron configuration has a high potential as a steady-state fusion reactor. © *2006 American Institute of Physics*. [DOI: 10.1063/1.2177204]

I. INTRODUCTION

The Large Helical Device (LHD) is a superconducting heliotron device that has continuous helical coils with $l=2$ and $m=10$.[1] Its nominal major and minor radii are 3.9 and 0.6 m, respectively. A magnetic field of 3 T is available for steady-state operation. It is the world's largest superconducting fusion device. A number of physics studies have been performed, and many technological achievements have also been reported for this device.[2–4] One of the main missions of the LHD is to develop the physics and technology for long-pulse or steady-state operation using an intrinsic helical divertor.[5,6] This mission is well suited to the LHD, because it is a heliotron device that does not require a plasma current for plasma confinement; it is also a superconducting steady-state device.

The structure of the magnetic configuration of the LHD is quite different from axisymmetric toroidal devices such as tokamaks, especially with regard to the outer region of the last closed flux surface. There is no clear separatrix, and the structure is characterized by the coexistence of a stochastic region, residual islands, whisker structure, a laminar region, and the intrinsic helical divertor. The helical divertor in the LHD has four divertor legs, as does the double-null poloidal divertor in tokamaks, although the poloidal component of the magnetic field is larger than the toroidal one in the divertor region, unlike the poloidal divertor in tokamaks.[7] The distribution of the particle and heat loads along the divertor traces is not uniform, and the distribution pattern can be significantly changed by small changes in the magnetic axis position.[5] During the long plasma operation period, the magnetic axis was slowly swung reciprocally in order to disperse the heat load along the divertor traces, and the maximum temperature of the carbon divertor plates was greatly reduced. This technique was first introduced into the LHD in the 2004 experimental program.

Using the LHD, we have tried steady-state operation over a period of 6 years using various heating devices: neutral beam injection (NBI), electron cyclotron (ECH), and ion

[a)]Paper FII 4, Bull. Am. Phys. Soc. **50**, 103 (2005).
[b)]Invited speaker. Author to whom correspondence should be addressed. Electronic mail: mutoh@nifs.ac.jp.
[c)]Also at Graduate University for Advanced Studies, Hayama 240-0163, Japan.
[d)]Also at Kyusyu University, Kasuga 816-8580, Japan.
[e)]Also at Nagoya University, Facultiy of Engineering, Nagoya 464-8601, Japan.
[f)]Also at Institute of Plasma Physics, Academia Sinica, Hefei 230031, P.R. China.
[g)]Also at Korea Atomic Energy Institute, Daejeon 305-600, Korea.

cyclotron range of frequencies (ICRF). The steady-state operation of the heating device is quite a difficult undertaking because the plasma-heating device was designed for high-power short-pulse operation with critical capacity. It is not optimized for long-pulse operation. Recently ECH heating devices[8,9] and ICRF[10,11] were developed for long-duration operation. In the last experimental program we used both ECH and ICRF devices continuously and NBI for periodic pulse operation. The successful long-pulse operation was undertaken to provide an understanding of the physics of divertor heating, device development, and innovative magnetic field operation techniques.

Before the LHD experiment, several tokamak devices had performed excellent long-pulse experiments. Tore Supra achieved operation for 6 min at 1.07 GJ,[12,13] TRIAM-1M achieved 5 h operation,[14] and JT-60U achieved 60 s operation. They all used the lower hybrid current drive (LHCD) technique. The requirement of a current drive technique to achieve long plasma operation is the most significant difference between heliotron devices and tokamaks.

II. HEATING DEVICES FOR STEADY-STATE OPERATION

In the LHD, long-pulse plasma operation was tried using three different heating techniques. Until 2003, NBI heating sustained plasma for 120 s, ICRF heating sustained it for 150 s, and ECH sustained it for 12 min for a plasma in the low-density range. All trials were done individually to test and develop hardware and operation techniques. Among these, the ICRF device was developed and prepared as the main steady-state heating technique, because it was the most realistic power source, maintaining a megawatt power level for more than 10 min.

Over the past 2 years the ICRF system in the LHD was reconstructed and improved to achieve reliable operation at high power for long periods. Many improvements in the transmitters, transmission lines, control systems, and loop antennas were carried out. In Fig. 1(a), the ICRF antennas and the LHD vacuum chamber are shown. The ICRF antennas are installed on the outer side of the torus at the vertically elongated sections, as seen in the figure.[15] For steady-state operation of the LHD, six antenna loops were installed. Four antennas were connected to transmitters through specially developed ceramic feedthroughs, coaxial lines, and liquid impedance tuners. Two antenna loops were not connected, but were prepared as spares for future programs.

The ICRF resonance and cutoff layers in the plasma cross section are shown in Fig. 1(b). The ICRF heating mode for the long-pulse experiment used minority ion heating with helium as the majority ions and hydrogen as the minority ions.[16] The ICRF antennas are located on the outer side of the toroid. Around this saddle point (marked as an X in the figure), the gradient of the magnetic field is very small, and increases towards the helical windings (left and right sides of the figure). The field decreases towards the divertor region (upper and lower sides). Strong cyclotron damping can be expected if the cyclotron resonance is located near the saddle point, as shown in the figure. Good ICRF-heating performance was obtained with this resonance location. The left-hand cutoff, and the two-ion hybrid resonance layers were located near the plasma axis for a majority helium concentration of 70% and minority proton concentration of 30%.

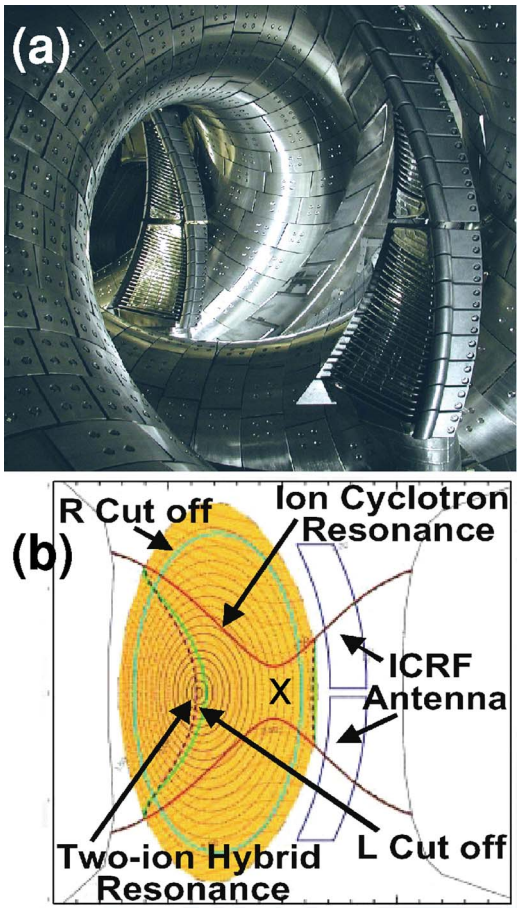

FIG. 1. (a) The inside of the LHD vacuum chamber. Helical coil cases and ICRF antennas can be seen. (b) Resonance and cutoff surfaces on the cross section LHD plasma at the vertically elongated section are shown. (Helium plasma with minority hydrogen: $n_H/(n_H+n_{He})=30\%$; axis electron density: $n_{e0}=1.0\times10^{19}$ m^{-3}; axis magnetic field strength: $B_0=2.75$ T; magnetic axis radius: $R_{ax}=3.6$ m; frequency: 38.47 MHz.)

In Fig. 2(a), one example of the results of the three-dimensional ICRF wave analysis calculation with the parameters for long-pulse operation is shown.[15] The calculation code was TASK-WM.[17] The results show that the deposition area of the ICRF wave is not central but near the saddle point of the mod-B surfaces. Most power is absorbed by the minority protons over a wide plasma-parameter range. This calculation is consistent with the experimental results.[15] Recently the TASK code was combined with the Monte Carlo orbit code for the LHD configuration, and it also predicts good performance when the resonance is located at the saddle point.

For the 2004 program, the ICRF antenna temperature was monitored by an infrared (IR) camera to allow optimization of the positions of the plasma axis and the antenna. The ICRF antennas were designed to move approximately 15 cm between the plasma and chamber wall to allow them to be set at the optimum position. During the plasma experiment, the carbon side protector of the antenna was locally

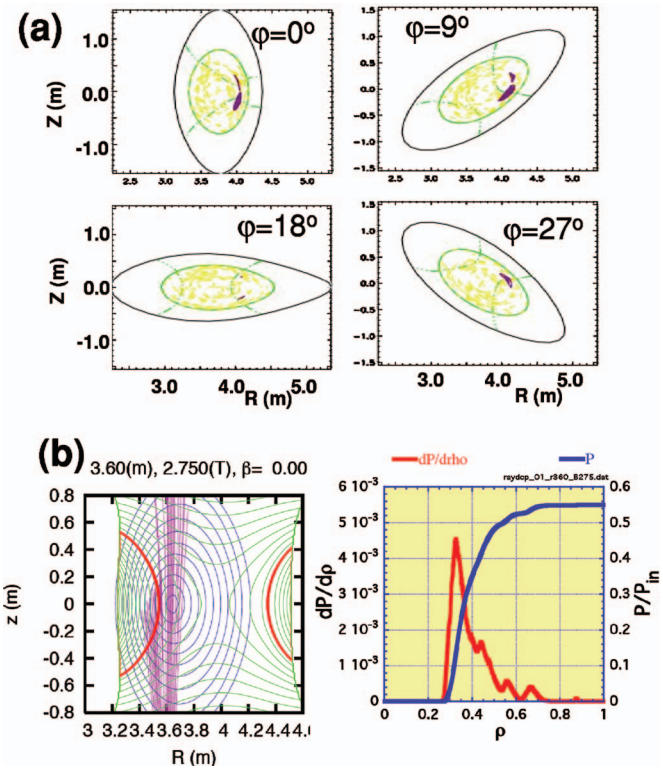

FIG. 2. (Color) (a) Calculation results of ICRF wave-damping analysis by the TASK-WM code for the conditions of long-pulse operation are shown. Contour plots of total absorbed power on the several plasma cross sections indicate that ICRF power is absorbed near the saddle point. The antenna is located at a toroidal angle of $\phi=0°$. The deposition pattern depends on both the wave field pattern and the cyclotron resonance layers. (b) Ray-tracing calculation of the ECH injection beam for a long pulse operation of 30 min. Around 50% of ECH power was absorbed by single pass absorption at 0.3–0.4 of the plasma radius. The residual part of the injected power is expected to absorb by multiple reflections at the chamber wall.

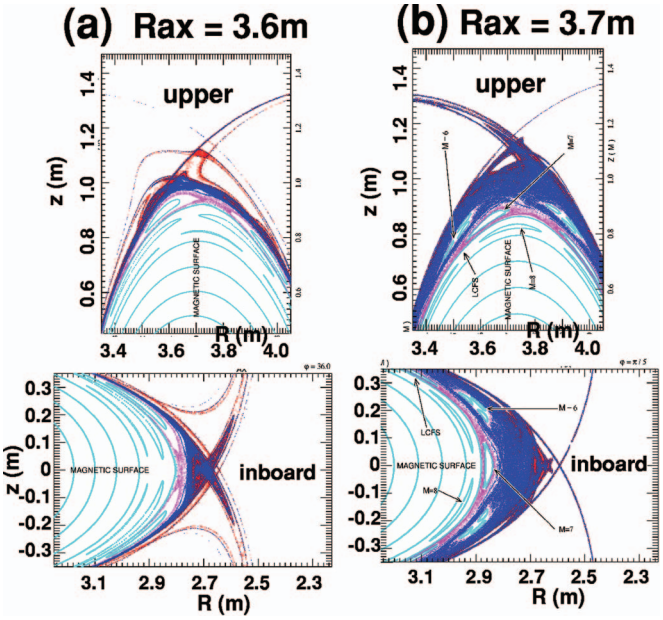

FIG. 3. (Color) Fine structure of the magnetic field near the divertor X point at vertically and horizontally elongated cross sections are shown for two magnetic-axis radius cases: $R_{ax}=3.6$ and 3.7 m.

heated if the antenna location was relatively close to the plasma. To avoid this local heating, the antennas were moved to the wall position, with the result that the plasma-coupling resistance decreased. The coupling resistance changed by a factor of approximately two by changing the antenna position from just outside the scrape-off layer (SOL) to the wall position. For long-pulse experiments of more than several minutes, the antenna was located near the chamber wall because the radiated power was set at a relatively low level of 200–300 kW per single loop, so that the radio frequency (rf) standing-wave voltage on the transmission line was at a low level of less than 25 kV_{0-p}.

Subsequent to the experimental program of 2003, a continuous wave (cw) ECH system began operation at the LHD. It successfully operated for 12 min with 100 kW injection power in 2003.[9] The ECH system was also improved, especially the transmission-line system, for a longer operation program. In the 2004 experimental program, the ECH 100 kW system and the ICRF 1000 kW system could be used simultaneously. The ECH power is not larger, but it has good plasma sustainment ability because it directly heats the electrons. In 2004, the ECH was able to sustain the plasma for more than 1 h at a power level of 110 kW, which is the duration record for plasma sustainment at LHD. The frequency of the ECH is 84 GHz, and it resonates at 3 T. Figure 2(b) shows the ECH ray-tracing calculation results for the conditions of the 30 min operation. This analysis uses realistic Gaussian multibeams from the waveguide antenna, which was used only for the long-pulse operation. Power deposition was located at approximately 0.4 of the plasma radius, and 55% of the power was absorbed by one-pass damping. The microwave beam was not focused in this case, but for short-pulse operation, it was strongly focused.

For the 30 min operation, repetitive NBI heating of 500 kW with 25 s pulses was also used as the auxiliary heating device.[18] This was especially important when the plasma axis shifted to the outer side, where the plasma density sometimes increased if the wall conditioning was not complete. Repetitive NBI heating was also useful to keep the minority proton ratio within a suitable range. We did not feed any hydrogen gas during the operation, with the consequence that the proton ion ratio was sometimes decreased to a level that was too low for operation times of more than several minutes.

III. DIVERTOR HEAT-LOAD AND MAGNETIC-AXIS SWING OPERATION

In the heliotron configuration, the intrinsic divertor structure is formed without any additional coils. The magnetic field structure in the LHD SOL is shown in puncture plots of the magnetic field lines in Fig. 3. Light blue lines show closed surfaces, while red and blue lines indicate the puncture points of the open field lines. There is no clear separatrix, and the residual islands with small poloidal mode numbers are in the sea of open field lines. Near the last closed flux surface (LCFS), there is the stochastic region.[7] Field lines in this region approach the LCFS, and are the main channel for particle and heat transport from the LCFS

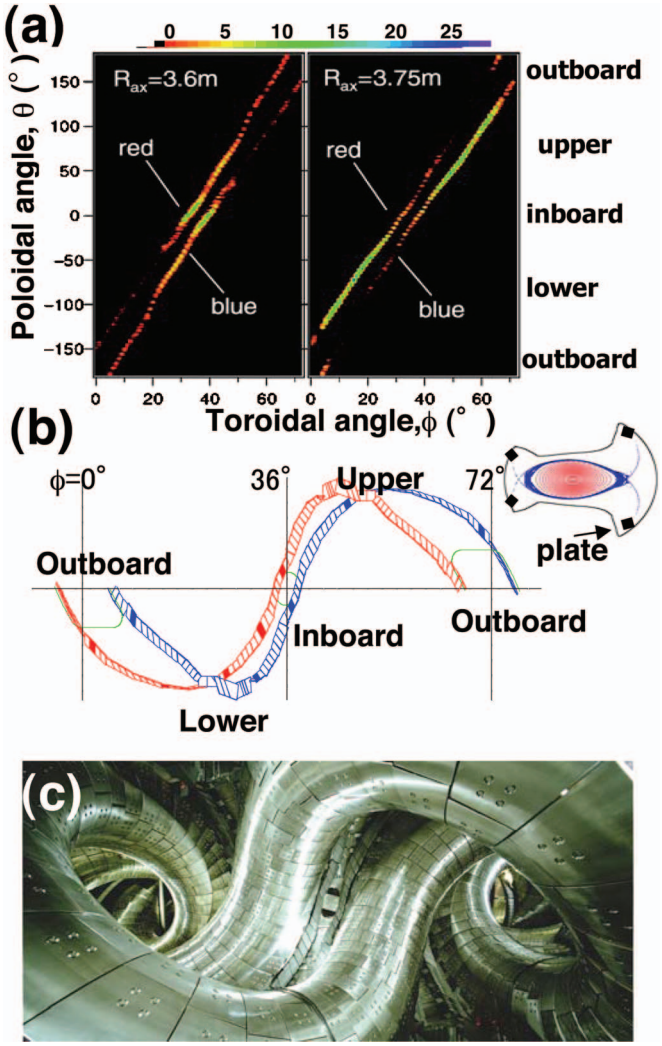

FIG. 4. (Color) (a) Contour plots of calculated particle deposition on the helical divertor traces in the toroidal and poloidal angle planes. (b) Schematic drawing of carbon plates along the divertor legs during one helical pitch. The filled colored plates are monitored by thermocouples. (c) Photo from inside the outboard port using a wide-angle camera. (From Ref. 5.)

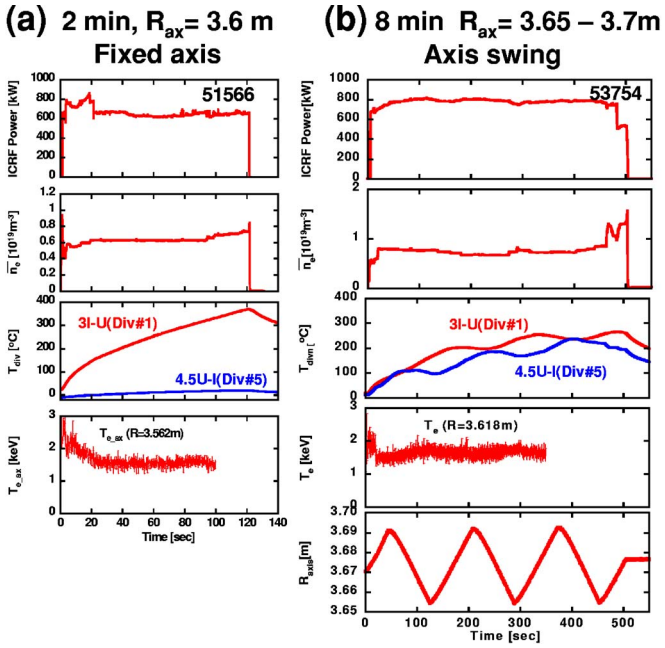

FIG. 5. Comparison between two discharges for the fixed-axis and swing-axis cases. (a) Temperature of one divertor plate in the fixed-axis case increases monotonically over 2 min and the plasma terminated. (b) In the swing-axis case, temperatures of plates stayed below 300 °C for a longer duration of 8 min.

to the divertor.[5] A connection length (L_c) for field lines longer than several hundred meters is a characteristic of this region. The whisker structure (or the edge surface layer) is well distinguished in the edge region of the SOL. There are laminar regions between the whiskers. The whiskers are drawn from the SOL to the divertor at the residual X points, and form the divertor legs. The magnetic structure in the SOL and the divertor are different for toroidal and poloidal locations, that is, the structure is three dimensional. The essential factor determining the profiles for particle and heat loads on the divertor is the local shear of the rotational transform near the residual X points.[6] This is determined by the operational magnetic configuration, such as the major radius of the magnetic axis (R_{ax}). As shown in Fig. 3, the thickness of the divertor legs is changed by changing R_{ax}. For the case of R_{ax}=3.6 m, the divertor legs are thicker at the inner side than at the upper side. In contrast, for the case of R_{ax}=3.7 m, there is a thick divertor leg at both the upper and lower sides. Thick divertor legs are considered to carry a large number of particles and a large amount of energy.

Field-line tracing that simulates the particle deposition pattern on the helical divertor plates by taking into account diffusion by a random walk process is shown in Fig. 4(a).[5] The contour plots of the number of field lines connected to the divertor plates are shown in the planes of the toroidal and poloidal angles. The left figure is for the case of R_{ax}=3.6 m, and the right figure is for the case of R_{ax}=3.75 m. The difference is obvious. The number of field lines is large at the inner side for the R_{ax}=3.6 m case, and for the top and the bottom divertor for the R_{ax}=3.75 m case, the number is large at both inboard sides of the torus. These results of the calculation are consistent with the experimental observations.[5,6]

The divertor-plate array in the LHD vacuum chamber is shown in Fig. 4(b), and a picture of the divertor-plate array in the LHD vacuum chamber, taken with a wide-angle camera, is shown in Fig. 4(c). Currently, the LHD divertor is an open configuration, but it is planned to install a baffle structure to form a closed-type divertor.[19] Some divertor plates shown in Fig. 4(b) are colored: thermocouples are installed inside these. In addition, Langmuir-probe electrodes are embedded in some plates to investigate the three-dimensional structure of the particle deposition pattern.[19]

Before the 2003 program, the plasma-sustainment time of the ICRF long-pulse experiment was limited by the temperature rise of the carbon divertor plates near the ICRF antenna, and the gradual increase in outgassing finally terminated plasma operation.[20,21] After that experiment, a new mechanical-joint type of divertor module and new carbon sheets were introduced to suppress the temperature rise and the outgassing of the carbon tiles. In addition, for the 2004

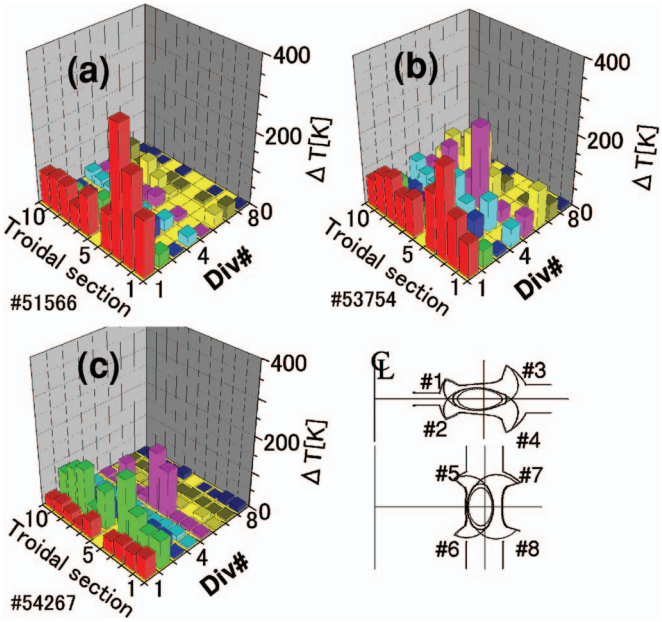

FIG. 6. (Color) Temperature rises of sampled divertor plates along the divertor legs for several discharges. (a) Fixed axis discharge of Fig. 5(a) (2 min, 100 MJ, R_{ax}=3.6 m fixed). (b) Swing-axis discharge of Fig. 5(b) (12 min, 400 MJ, R_{ax}=3.63–3.67 m). Heat deposition was well dispersed along the divertor traces. (c) Fixed axis discharge with reversed magnetic field. Heat deposition was changed from Div#1 to Div#2 (80 s, 70 MJ, R_{ax}=3.6 m, B direction was reversed).

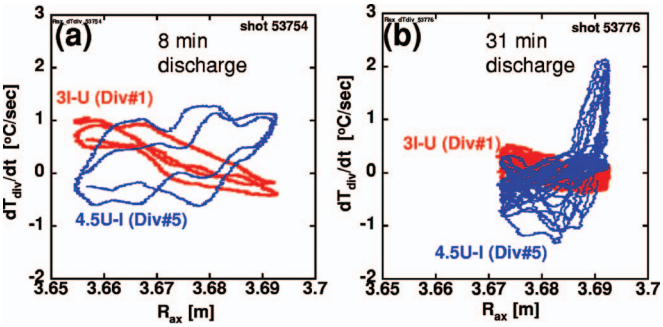

FIG. 7. (Color) Lissajous figures of the divertor heat load and magnetic axis radius are shown for two long-pulse discharges. (a) is for the same plasma shown in Fig. 5(b); (b) is for the 31 min operation with a narrow axis swing range between 3.67 and 3.7 m. Steep peaks at near R_{ax}=3.69 m are because of the repetitive NBI injections.

experimental program, an innovative technique was introduced: a real-time R_{ax} swing by controlling the vertical magnetic field. This technique successfully dispersed the divertor heat load. This idea is based on an understanding of LHD divertor physics mentioned above.

Figure 5 shows a comparison of two plasma discharges. The left side shows the plasma parameters for the case of fixed R_{ax} operation (R_{ax}=3.6 m), and the right figure shows the case for a discharge with R_{ax} swing (R_{ax}=3.65 −3.70 m). The input ICRF power and plasma density are almost the same in both cases. For the case of the fixed R_{ax} discharge, the temperature of the inner divertor plate increased monotonically during ICRF injection, and it reached approximately 400 °C after 120 s. The temperature of the top divertor plate remained low. This is consistent with the calculation result of Fig. 4(a). On the other hand, in the discharge with R_{ax} swing, both the inner and top divertor plates were heated, but their temperatures did not monotonically increase. The heat load was reduced below the cooling capability of the carbon divertor plates for a period of 500 s.

The distribution of the ICRF heat load was not uniform in the toroidal direction. Roughly sampled temperature measurements of the divertor plates are shown in Fig. 6. The ICRF antennas are located at toroidal sections 3.5 and 7.5. More than 70% of the power was injected from the 3.5 antennas. For a fixed R_{ax} of 3.6 m [Fig. 3(a)] temperatures at position Div#1 (divertor leg of No. 1), especially near the 3.5 ICRF antennas, were noticeably locally heated. By using the R_{ax} swing technique, this poloidal local heating was largely dispersed, as shown in Fig. 6(b). Peak temperature increments were reduced to less than 300 °C after 500 s operation, although the toroidal local heating near the 3.5 antennas still remained.

Asymmetry of the heat load on the divertor plates at the geometrical symmetric positions Div#1 and Div#2, is observed in Figs 6(a) and 6(c). Case (c) is for the reverse magnetic field direction. This discharge is of short duration and the input energy is relatively small. For the field-line calculation shown in Fig. 4(a), there is no asymmetry between Div#1 and Div#2. The observed asymmetry is probably explained by particle transport near the residual X points. If the $\mathbf{B}\times\nabla\mathbf{B}$ drift (where $\mathbf{B}$ is the static magnetic field vector) is relatively large at the residual X points, the particle flow rate can be affected by drift motions. The reverse tendency for the opposite field direction [case (c)] is consistent with this explanation. The high-energy particles accelerated by the ICRF electric field can also be affected by this drift motion.

During the R_{ax} swing operation, the temperatures of Div#1 and Div#5 changed almost out of phase with the frequency of the axis swing. The behavior of the divertor heat load can be investigated from the temperature change of these tiles. Figure 7 shows a Lissajous figure using temperature derivatives of the two tiles and the magnetic axis radius for the discharge of Fig. 5(b) during a 30 min operation discharge. In the left figure, the heat load to Div#1 (inner-side tile) shows a monotonic dependence on the magnetic axis position, and the heat load to Div#5 (top-side tile) shows an inverse tendency. A somewhat early phase shift was observed in Div#5; however, the reason for this is not clear. During the 30 min operation (right-hand figure), the tile temperatures showed a similar behavior. The steep temperature rise of Div#5 for large R_{ax} was because of additional neutral beam injections.

Using the R_{ax} swing technique, the particle deposition profile on one divertor tile was also effectively dispersed. Langmuir-probe arrays were embedded in several tiles, and the ion saturation current profile was measured.[19] In Fig. 8, time traces of contour plots of the ion saturation current at the inner and bottom divertor tiles are shown. One of them is located on a divertor tile of Div#1 positioned at the inboard side of the torus, and another one is located on a divertor tile of Div#6. The positions are explained in Fig. 6. The upper figures are for a fixed R_{ax} discharge, and the lower figures are

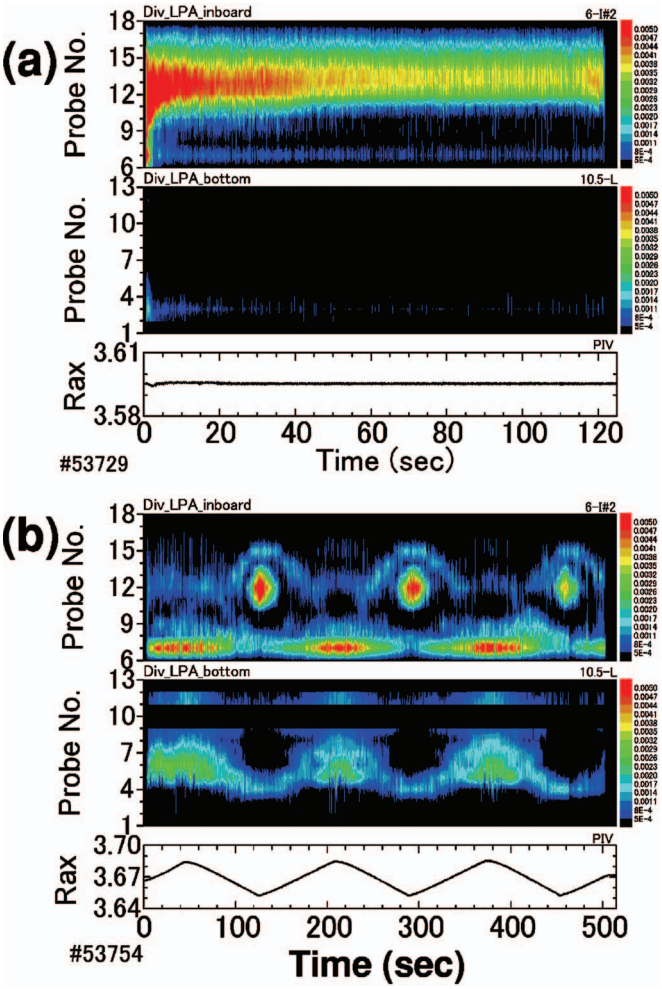

FIG. 8. (Color) Contour plots of the ion saturation current of the Langmuir-array probes embedded in the divertor plates. The upper and lower plots correspond to two divertor traces on the inboard side at the horizontally elongated section. (Places embedded are at #1 and #2 shown in Fig. 6.) (a) is for the case of a fixed axis position of R_{ax}=3.6 m, and a pulse length of 2 min; (b) is for the swung axis case of Fig. 5(b).

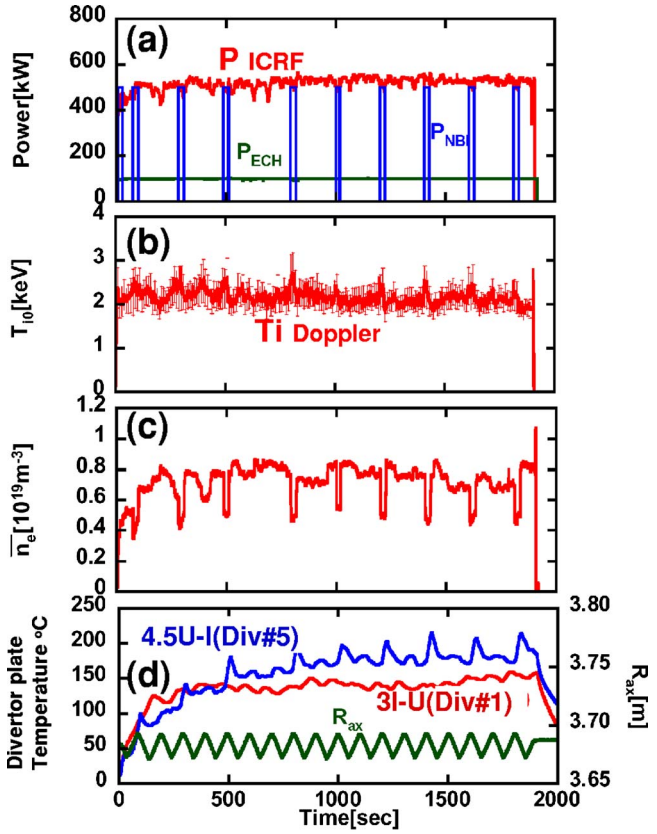

FIG. 9. Plasma parameters for the 31 min operation are shown: input power of ICRF, ECH, and NBI, ion temperature by Doppler measurement, line-averaged electron density, temperature of divertor plates, and magnetic axis radius (reciprocally swept). (#53766, He, 2.75 T at R=3.6 m).

for the R_{ax} swing discharge of Fig. 5(b). This figure shows that the axis swing can disperse the particle flux on each divertor tile. The distance between probe tips is 6 mm, and the tips are along the edge of the divertor plates.[19]

These results show that the R_{ax} swing technique is quite effective in dispersing the divertor heat load at both macroscopic (along the divertor plates array) and microscopic (on a divertor plate) levels. This new technique allowed us to achieve the long plasma sustainment time.

In this paper, we used several cases of R_{ax} swing range to explain the divertor characteristics. 30 min operation was achieved for the axis swing range between 3.67 and 3.7 m. The calculation in Fig. 3 shows a clear difference in the divertor field structure between 3.6 and 3.7 m. The experiment used this structure difference effectively. Figure 4 is taken from Ref. 5 (Masuzaki *et al.*), which showed the typical LHD configurations frequently used in LHD experiments. This is also a typical explanation of standard and inward shifted configurations. Figures 5(b) and 8 show the data for the case without NBI injections. We have a small data base for without NBI injection. With NBI injection, the data are noisy and complicated to explain.

IV. STEADY-STATE OPERATION FOR 30 MIN

The steady-state operation with the R_{ax} swing was performed under standard experimental conditions in the LHD. The magnetic axis radius was swung between 3.67 and 3.7 m, the magnetic strength was 2.75 T at R_{ax}=3.6 m, and the pitch parameter of the helical winding was 1.245. The helical coil current was kept fixed, and the vertical coil currents were changed. Three ICRF antenna loops were used, and the frequency was 38.47 MHz. Under these conditions, the cyclotron resonance region of the minority ions was located near the saddle point on the mod-B contour plane in the cross section of the plasma. In this mode, the ICRF wave power heated the minority ions, but did not heat the electrons directly. Therefore, the bulk plasma was heated by relaxation from the high-energy component of the minority protons to the electrons and ions. For an ECH of 84 GHz, the cyclotron-resonant layer was not on the plasma axis but at approximately 0.4 times the radius of the plasma. The LHD vacuum chamber was conditioned by boronization, which seemed to be effective in keeping the impurity influx at low levels during steady-state operation.

Time traces of the plasma parameters are shown in Fig. 9. The ICRF and ECH were injected continuously, and NBI

was repetitively injected by 25 s pulse operations, as shown in Fig. 9(a). The plasma was sustained mainly by ICRF and supported by ECH and NBI. The average power was 520 kW by ICRF, 100 kW by ECH, and 60 kW by NBI. The total input energy to the plasma reached 1.3 GJ. The ECH and NBI components helped to sustain the plasma during some disturbances; for example, occasional metal flakes dropping from the vacuum vessel.

NBI pulses were repetitively injected when the plasma was located at the outer major radius position near where the plasma and antenna/wall interaction was strong. Another role of NBI was to feed hydrogen to the plasma by the injected beam. Without beam heating, the spectrum line ratio of $H\alpha$: HeI monotonically decreased. The proper range of the proton ion to helium ion ratio was around 5%–30% in LHD ICRF heating. The NBI pulse helped to maintain the proper ratio during long-pulse operation without any hydrogen gas puffing. The power and pulse length of NBI heating was limited by the cooling capacity of the NBI system.

During the 31 min discharge, helium gas was fed by a puffing system to form the majority-ion species for ICRF heating. The repetitive NBI pulses acted to heat the plasma and also to keep the hydrogen concentration ratio within a suitable range for the minority-heating mode of the ICRF. The central ion temperature (measured by Doppler broadening of the Ar XVII line) was approximately 2 keV or higher [Fig. 9(b)], and the line-averaged electron density was approximately $0.7-0.8\times10^{19}$ m^{-3} [Fig. 9(c)]. During the NBI heating phases, the electron density dropped by about 30% because of the change in particle confinement time and the recycling rate. The electron temperature was almost the same as the ion temperature.

The long-duration operation was made possible by introducing the swing technique. During the operation, the R_{ax} swing was performed 18.5 times between 3.67 and 3.7 m, as shown in Fig. 9(d). The time variation of the temperature of the inner (Div#1 in Fig. 6) and upper (Div#5) tiles is shown in Figs. 7(b) and 9(d). These figures show the expected out-of-phase temperature changes of these divertor plates. During the 30 min discharge, the R_{ax} swing operation worked very well, and kept the divertor tile temperature within a reasonable range.

Figure 10(a) shows a video frame of the LHD plasma 30 min after the start, and the temperature of the divertor tiles at the end of 31 min of operation. On the video frame, there is a hot spot indicated by a circle. This location was a carbon protector edge of the ICRF antenna. This hot-spot temperature was measured by an IR camera and was affected by the R_{ax} swing. When R_{ax} and the plasma boundary moved to the outer side, the hot-spot temperature increased; in contrast, it decreased for the opposite motion. The reason for the hot spot is not yet clear. One possibility is that high-energy ions circulated just outside the closed magnetic surfaces, and another possibility is a local rf field effect that caused local heating because of the presence of the low-density plasma.

During the conditioning phase, the plasma duration increased shot by shot. Usually, the plasma suddenly terminated when R_{ax} moved to the outer side. The hot spot of the ICRF antenna protector seemed to be one of the causes of

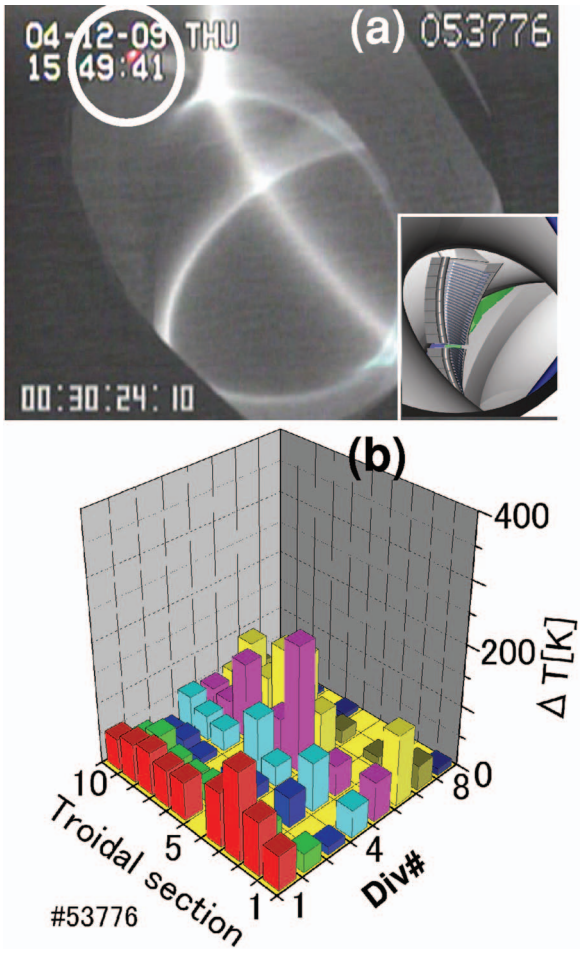

FIG. 10. (Color) (a) A video frame of a plasma observed from a horizontal port 30 min after the start. A hot spot on the antenna edge is indicated by a circle. The brightness changed according to the axis swing motion. Antennas and vacuum chamber positions are shown by a CAD drawing in the small rectangle. (b) The divertor tiles' temperature at the end of 31 min operation.

plasma termination. This is the reason that an additional NBI pulse was superposed when the plasma was located near the outer turning point of the R_{ax} swing motion, as shown in Figs. 7(b) and 9.

The temperature of the divertor tiles after 31 min generally stayed below 300 °C [Fig. 10(b)]. This shows that heat dispersion along the divertor traces was satisfactory during the long operation period.

The discharge shown in Fig. 9 was terminated because of a sudden increase in plasma density and an increase in radiation power that coincided with a sudden increase in the intensity of the iron-impurity line. We presume that melted metal or metal flakes dropped into the plasma and terminated the operation. The origin of the metal impurity was not found during an inspection of the vacuum chamber after the experimental program. Before this experimental program, the long-pulse operation using ICRF was terminated by a gradual increase in electron density and radiation loss several minutes after the inception of plasma. The electron density became uncontrolled and exceeded the density limit of ICRF operation. This uncontrollability was overcome by introducing the real-time axis swing technique discussed in this paper. Metal

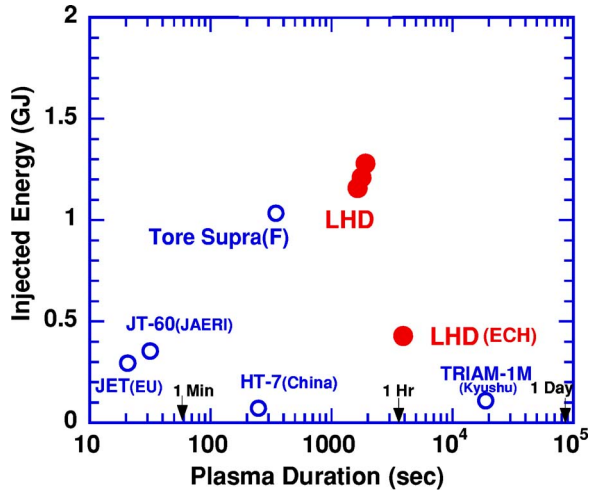

FIG. 11. Maximum injected energies of major steady-state or long-pulse operation devices are plotted versus plasma confinement time. The LHD has extended the envelope of long-pulse plasma experiments.

impurity is the main problem that needs to be solved in the next experimental program.

V. HIGH-INPUT ENERGY TO PLASMA

Long-pulse operation of a high-temperature plasma is one of the main topics in the world of large fusion experimental devices. Commercial fusion reactors should work continuously and long plasma sustainment is a necessary requirement of a fusion reactor device. Long-duration discharges achieved to date are plotted on the plane of total input energy and plasma-duration time in Fig. 11. Data for other major devices that have achieved steady-state operation or a relatively long-pulse high-power operation are also shown. Tore-Supra, HT-7, and TRIAM-1M are superconducting tokamak devices that have sustained plasma for more than 1 min. The 1.3 GJ energy of the LHD is the highest input energy for high-temperature plasmas at keV levels for any magnetic confinement device, including tokamaks and helical devices.

It should be remembered that the LHD is a heliotron-type device and does not require plasma current for confinement, as do tokamaks. This is a logical reason for the achievement of this long operation time. In addition, this plasma was heated and sustained mainly by the ICRF minority ion-heating mode, which produces high-energy ions that are easily trapped by magnetic field ripples. These results show that the heliotron configuration has a high potential as a steady-state fusion reactor.

ACKNOWLEDGMENTS

The authors wish to thank the technical staff of the LHD group at the National Institute for Fusion Science for their helpful support during this work.

This work was partially supported by NIFS code of NIFS05ULRR001, 504.

[1] O. Motojima, K. Akaishi, H. Chikaraishi *et al.*, Nucl. Fusion **40**, 599 (2000).
[2] O. Motojima, H. Yamada, A. Komori *et al.*, Fusion Sci. Technol. **46**, 1 (2004).
[3] S. Sudo, Y. Nagayama, M. Emoto *et al.*, Rev. Sci. Instrum. **72**, 483 (2001).
[4] A. Komori, N. Ohyabu, H. Yamada *et al.*, Plasma Phys. Controlled Fusion **45**, 671 (2003).
[5] S. Masuzaki, T. Morisaki, N. Ohyabu *et al.*, Nucl. Fusion **42**, 750 (2002).
[6] T. Morisaki, S. Masuzaki, M. Goto *et al.*, Contrib. Plasma Phys. **42**, 321 (2002).
[7] N. Ohyabu, T. Watanabe, H. Ji *et al.*, Nucl. Fusion **34**, 387 (1994).
[8] S. Kubo, Y. Yoshimura, T. Shimozuma *et al.*, AIP Conf. Proc. 16th Topical Conference on Radio Frequency Power in Plasmas, Park City, Utah, 2005 (American Institute of Physics, 2005), AIP Conference Proceedings 787, p. 411. 787, 411 (2005).
[9] K. Ohkubo, S. Kubo, R. Kumazawa *et al.*, *Proceedings of the 20th IAEA Fusion Energy Conference*, Vilamoura, Portugal, 2004 (IAEA, Vienna, 2004), IAEA-CN116/FT/P7-19.
[10] T. Mutoh, R. Kumazawa, T. Seki *et al.*, Nucl. Fusion **43**, 738 (2003).
[11] R. Kumazawa, T. Mutoh, T. Seki *et al.*, Phys. Plasmas **8**, 2139 (2001).
[12] D. van Houtte, G. Martin, A. Becoulet *et al.*, Nucl. Fusion **44**, L11 (2004).
[13] J. Pamela, E. R. Solano, and JET EFDA Contrib., Nucl. Fusion **43**, 1540 (2003).
[14] H. Zushi, K. Nakamura, K. Hanada *et al.*, Nucl. Fusion **45**, S142 (2005).
[15] T. Mutoh, R. Kumzawa, T. Seki *et al.*, Phys. Rev. Lett. **85**, 4530 (2000); R. Kumazawa, T. Mutoh, T. Seki *et al.*, J. Plasma Fusion Res. **3**, 352 (2000). T. Seki, R. Kumazawa T. Mutoh *et al.*, J. Plasma Fusion Res. **5**, 478 (2002). K. Saito, R. Kumazawa, T. Mutoh *et al.*, Nucl. Fusion **41**, 1021 (2001).
[16] T. Mutoh, R. Kumazawa, T. Seki *et al.*, J. Plasma Fusion Res. **81**, 229 (2005).
[17] A. Fukuyama, E. Yokota, and T. Akutsu, *Proceedings of the 18th IAEA Fusion Energy Conference*, Sorrento, Italy, 2000 (IAEA, Vienna, 2000), IAEA-CN77/THP2/26.
[18] Y. Takeiri, Y. Nakamura, N. Noda *et al.*, Plasma Phys. Controlled Fusion **42**, 147 (2000).
[19] S. Masuzaki, T. Morisaki, M. Shoji *et al.*, "Overview and future plan of helical divertor study in the Large Helical Device," to be published in Fusion Science and Technology.
[20] T. Mutoh, R. Kumazawa, T. Seki *et al.*, Fusion Sci. Technol. **46**, 175 (2004).
[21] R. Kumazawa, T. Mutoh, K. Saito *et al.*, Nucl. Fusion **46**, S13-S21 (2005).